Published in final edited form as:
Trends Biotechnol. 2010 February ; 28(2): 93–101. doi:10.1016/j.tibtech.2009.11.004.

Musculoskeletal molecular imaging: a comprehensive overview

Marie K. Reumann, **Mitchell C. Weiser**, and **Philipp Mayer-Kuckuk**
Bone Cell Biology and Imaging Laboratory, Caspary Research Building, Rm. 623, Hospital for Special Surgery, 535 East 70th Street, New York, NY 10021, USA

Abstract

Molecular imaging permits non-invasive visualization and measurement of molecular and cell biology in living subjects, thereby complementing conventional anatomical imaging. Herein, we review the emerging application of molecular imaging for the study of musculoskeletal biology. Utilizing mainly bioluminescence and fluorescence techniques, molecular imaging has enabled *in-vivo* studies of (i) the activity of osteoblasts, osteoclasts, and hormones, (ii) the mechanisms of pathological cartilage and bone destruction, (iii) skeletal gene and cell therapy with and without biomaterial support, and (iv) the cellular processes in osteolysis and osteomyelitis. In these applications, musculoskeletal molecular imaging demonstrated feasibility for research in a myriad of musculoskeletal conditions ranging from bone fracture and arthritis to skeletal cancer. Importantly, these advances herald great potential for innovative clinical imaging in orthopedics, rheumatology, and oncology.

Introduction

Molecular imaging is defined as the non-destructive, *in-vivo* visualization and measurement of biology at the molecular and cellular level [1–4]. The emergence of non-invasive imaging of biological processes has profound implications in pre-clinical research because it provides, for the first time, the opportunity to make discoveries directly in living, intact tissue. Molecular imaging is expected to affect subsequent clinical imaging through earlier and more accurate diagnosis of disease. Musculoskeletal molecular imaging is the specific application of molecular imaging to the hard and soft tissues of the musculoskeletal system. In this contribution, the expanding field of musculoskeletal molecular imaging is reviewed, from its use in endogenous bone cell biology to its application toward assessing cellular responses to exogenous biomaterials.

Imaging the activities of osteoblasts, osteoclasts, and hormones

Osteoblast activity

In pioneering studies, Gazit *et al*. described the *in-vivo* imaging of bone-forming osteoblasts [5,6], thereby providing an early example of molecular imaging in musculoskeletal tissue (Box 1). They hypothesized that *Firefly* luciferase (FLuc) expression from the osteoblast-specific osteocalcin (OC) promoter could be monitored non-invasively in bone tissue of living mice. The principle of using luciferases such as FLuc for bioluminescence imaging is illustrated in Figure 1. To test their hypothesis, Gazit *et al*. generated a transgenic mouse model harboring FLuc under the control of an OC promoter fragment. Light emission from the OC -FLuc animals correlated with the activity of osteoblasts and hypertrophic chondrocytes in the tail vertebrae, calvaria, carpals and tarsals as well as the spine (Figure 2a), thus matching well with the expected pattern of OC expression [6]. Imaging could

Corresponding author: Mayer-Kuckuk, P. (mayerkuckukp@hss.edu).

reveal the developmental expression of osteocalcin in these tissues. In non-stabilized radial defect and bone-marrow ablation models, bioluminescence imaging identified the *in-vivo* time-course and peak of osteocalcin expression post-damage [6]. Together, the OC-FLuc mouse offered specific measurement of OC expression *in vivo*. This model could be used to study molecular mechanisms in skeletal gene and cell therapy (as described below) and has helped to define musculoskeletal molecular imaging (Box 2).

Box 1

Musculoskeletal biology and the *rationale* for molecular imaging

The musculoskeletal system constitutes various specialized tissues, including bone, tooth, cartilage, tendon/ligament, and skeletal muscle. These tissues are formed by cells of mesenchymal origin, such as osteoblasts, odontoblasts, chondrocytes, tenocytes/ligament cells, and skeletal myocytes, respectively. The current view is that postnatally most of the musculoskeletal mesenchymal cell types form from the mesenchymal stem cell (MSC) via a controlled sequence of proliferation, commitment and differentiation [75,76]. Cell populations characterized as MSCs have been isolated from many adult tissues, but the precise identity of the MSC remains elusive. Unique to bone and calcified cartilage is the existence of a tissue-degrading cell, the osteoclast, which derives from the hematopoietic stem cell. The bone-forming osteoblast and bone-resorbing osteoclast lineages are connected through various functional convergence points; most prominently, receptor activator for NF- κB (RANK) and its ligand (RANKL). Hence, the formation and resorption of bone during initial formation (modeling), as well renewal in the course of life (remodeling), are tightly coupled.

The structural support, motor function, and metabolic activity provided by musculoskeletal tissues are strictly dependent on their integrity. Thus, studying living, intact tissues in animal models is essential for musculoskeletal research. Histology is a superb method for the analysis for animal models, but is associated with (i) restriction to *post-mortem* evaluation, (ii) sample analysis under non-physiological conditions, (iii) labor-intensive tissue sampling that is subject to variability, and (iv) a time lag between sampling and evaluation of tissue. Molecular imaging can circumvent these shortcomings through direct analysis in living subjects (Figure I). As such, it complements anatomical imaging by providing a ‘biological read-out’.

To image a biological constituent or activity *in vivo*, it must possess a specifically detectable property. Most macromolecules and cells do not exhibit intrinsic properties that would permit detection with currently available imaging. Molecular imaging is therefore regularly carried out in two sequential steps. Imaging visibility is first conferred on an *in-vivo* constituent or activity (Figure 1). This is followed by the imaging process, which employs an external imaging device that allows an observer to ‘see’ the constituent or activity within the body. By comparison, individual imaging modalities have distinct application characteristics (Table 1).

Box 2

A brief history of molecular imaging

The development of molecular imaging is rooted in radiology and nuclear medicine as well as in molecular biology. Since the 1950s, nuclear imaging of radioactive isotope-labeled biomacromolecules has been an integral part of drug development and diagnostic imaging. The broad clinical significance of such approaches remained restricted until positron emission tomography of fluorine-labeled 2-fluorodeoxy-D-glucose was

introduced in 1979, and became an important tool for the detection of metabolic activities in tissues such as the brain and heart, as well as in cancer. It facilitated a biological imaging read-out, albeit with limited specificity. Around the same time, magnetic resonance spectroscopy promoted the evolution of molecular imaging. The ability to collect information about specific endogenous molecules by taking advantage of their intrinsic nuclear spin property represented an early example of molecular imaging. These advances paved the way for pioneering molecular imaging studies by demonstrating *in-vivo* imaging of reporter gene expression [77,78]. Concurrently, optical bioluminescence imaging for *in-vivo* detection of the FLuc reporter gene was demonstrated [79]. Taken together, these studies propelled molecular imaging into the scientific spotlight. The introduction of imaging instrumentation dedicated to small animals [80] and the description of enzyme-activated small-molecule probes for optical fluorescence imaging further fueled scientific interest [81]. Recent work has focused on the extension and refinement of molecular imaging technology and its application to the diagnosis of cancer [82] and cardiovascular disease [83]. Molecular imaging has started to emerge as a tool in immunology [84], microbiology [85], and orthopedics [86–88].

Bone-seeking nuclei and compounds have established clinical applications. For example, fluorine-18 and radiolabeled methyl diphosphate are imaging tracers, whereas bisphosphonates are a class of drugs that inhibit bone resorption. Assuming uptake in areas of exposed bone mineral, these nuclei and compounds can be used as surrogate markers for the activity of osteoblasts and osteoclasts. Recent work by Silva *et al.* re-visited positron emission tomography (PET) of fluorine-18 for assessment of damage- and time-dependent responses to fatigue loading in living rats [7]. For optical imaging applications, Zaheer *et al.* introduced the bisphosphonate pamidronate covalently coupled to a near-infrared (NIR) fluorophore [8]. The approach of using static probes for fluorescence imaging is illustrated in Figure 1. The authors studied skeletal concentration of the fluorescent pamidronate in juvenile nude mice. Whole-body fluorescence imaging displayed numerous bone structures in the skeleton. In subsequent work, Kozloff *et al.* validated imaging of osteoblast activity using NIR fluorophore-tagged bisphosphonate in a study employing fluorescence molecular tomography (FMT) [9].

Osteoclast activity

Kozloff and co-workers also described *in-vivo* imaging of osteoclast activity [10]. They utilized a NIR fluorophore-labeled probe that gained its fluorescence through enzymatic cleavage by cathepsin K (a well-characterized marker for osteoclasts) (Figure 1). The probe was administered to mice that underwent a sham-operation, ovariectomy for induction of osteoclast-mediated bone resorption, or ovariectomy plus anti-resorptive bisphosphonate treatment. Changes in osteoclast activity were successfully registered by FMT. By combining the earlier reported NIR fluorophore-tagged bisphosphonate with the cathepsin K-activated probe, parallel imaging of the activity of osteoblasts and osteoclasts was achieved. Imaging showed that after ovariectomy osteoclasts returned to normal activity earlier than osteoblasts. The studies of Kozloff *et al.* on osteoclast activity followed work by Sprague *et al*. which exploited $\alpha_v\beta_3$ integrin expression as a marker for osteoclast presentation [11]. Integrated PET/computed tomography (CT) imaging (Box 3) of isotope-labeled RGD peptide, a static probe (Figure 1), could detect drug-induced osteoclastogenesis in the calvarium. Overall, one can speculate that concurrent imaging of the activity of osteoblasts and osteoclasts has clinical potential in the diagnosis of bone disorders characterized by altered bone turnover (e.g., Paget's disease of bone or osteoporosis).

Box 3

Integrated anatomical and molecular imaging

The accuracy of imaging a biological constituent or activity in musculoskeletal tissues is determined not only by the imaging specificity and sensitivity, but also by the ability to map the signal *in vivo*. Many of the first-generation molecular imaging tools, including reporter gene-based bioluminescence and PET imaging as well as fluorescence imaging of probes and antibodies, have been developed for the visualization of biology and do not provide much anatomical information. Interpretation of molecular imaging data remains, in most cases, dependent on *post-mortem* tissue analysis. This holds true for almost all of the musculoskeletal imaging presented in this review. To circumvent this limitation, two main modes of integration for anatomical imaging such as conventional MRI, CT or ultrasound are under investigation. First, molecular and anatomical information can be acquired on separate instruments with subsequent image co-registration. The advent of pre-clinical and clinical hybrid modality instruments, for example PET –CT, SPECT–CT or PET–MRI, makes this approach increasingly effortless. [89]. Second, a single imaging modality can be used to monitor biology and anatomy; examples include proton MRI of iron oxide particle-labeled cells and ultrasound imaging of microbubble-tagged probes or antibodies. Photoacoustic imaging, which is based on ultrasound detection of transient thermal expansion post-light excitation, permits direct integration of conventional ultrasound imaging. Taken together, multimodality imaging is feasible and greatly improves imaging accuracy and interpretation. Its extended application to musculoskeletal imaging is foreseen. Musculoskeletal imaging is dominated by optical imaging, and this modality can be considered least precise in signal detection due to intrinsic limitations in light absorption and scattering in tissue. That is, multimodality imaging has limitations. Nevertheless, innovation in molecular imaging technology is likely to minimize or overcome many of these limitations, and will remain the driving force behind advances in musculoskeletal molecular imaging.

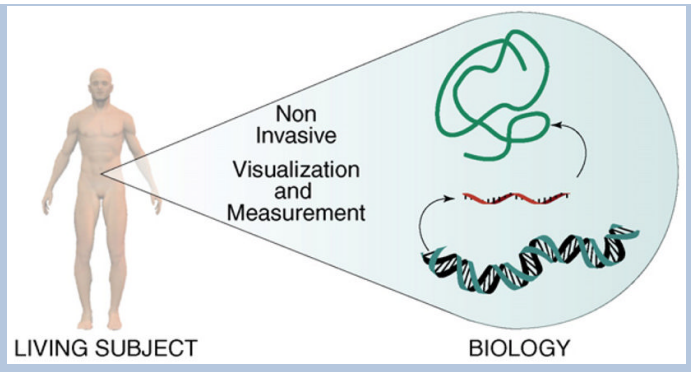

Figure I.
The principle of molecular imaging.

Hormonal activity

Osteoblasts and osteoclasts are subject to hormonal regulation. An example of how hormone action can be studied *in vivo* is the work by Ciana *et al.*, who generated transgenic mice carrying FLuc under control of an estrogen-responsive promoter [12]. Although the imaging reporter gene did not show tissue- nor cell-type specificity, it allowed, in combination with tissue analysis, the study of bone in juvenile mice [13]. The authors reported that, in immature or adult cycling mice, estrogen receptor activity in non-reproductive tissues (including bone) was partly estrogen-independent.

Imaging of mechanisms in pathological cartilage and bone destruction

Imaging of musculoskeletal destruction has focused on joint conditions such as rheumatoid arthritis (RA) or osteoarthritis (OA), but a significant body of work has also been directed toward the *in-vivo* biology of skeletal malignancies.

Arthritic inflammation

The development of transgenic reporter gene animals for bioluminescence imaging of gene expression in inflammation led to several studies demonstrating the feasibility of quantitative, longitudinal observations in models of RA [14–16]. Zhang *et al.* described mice expressing FLuc under control of a promoter for nitric oxide synthase or serum amyloid A 1 protein [14,15]. Imaging demonstrated a rapid induction of both promoters within hours after arthritis initiation. Work by Carlsen *et al.* introduced a mouse modified to express FLuc under control of three nuclear factor kappa B (NF- κB) sites [16]. Imaging in arthritic joints revealed a strong activation of NF- κB on day-6 post-arthritis induction and increased expression over the following four days [16]. Taken together, these studies emphasize the strength of luciferase reporter gene mice for quantitative longitudinal studies.

The trafficking of inflammatory cells in the arthritic joint was examined in several imaging studies [17–26]. Two groups investigated type-II collagen-specific $CD4^+$ T-cell hybridomas for delivery of interleukin to an inflammatory mouse joint [22,24]. The capacity of bioluminescence imaging for monitoring the biodistribution of lymphocytes modified to express FLuc in conjunction with a therapeutic gene was demonstrated. With the intention to offer two imaging modalities for visualization of a single target, a recent study described a T-cell hybridoma expressing a dual reporter construct containing *Renilla* luciferase and *Herpes simplex* virus 1 thymidine kinase (HSV1 TK) [26]. The modes of imaging using these reporter genes are outlined in Figure 1. To confer imaging visibility without the need for gene transfer, several research groups took advantage of the observation that activated

synovial macrophages overexpress a nonepithelial isoform of the folate receptor [27]. They used isotope and NIR fluorophore-conjugated folates to demonstrate the feasibility of imaging of macrophages infiltrating into inflamed joints [18,25,28]. Notably, in the NIR fluorescence imaging study, folate accumulation was detected before the development of visible signs of arthritis, suggesting the potential for early diagnosis (Figure 2b) [18]. In an alternate approach, Hansch *et al.* demonstrated macrophage imaging utilizing a NIR fluorophore-conjugated antibody directed against the macrophage antigen F4/80 [20] (Figure 1). More recently, Simon *et al.* presented optical imaging of joint infiltration of NIR fluorophore-labeled leukocytes in a rat model [23]. These studies were accompanied by clinical research that suggested the potential for targeted RA imaging agents using antibodies or probes [29]. NIR optical imaging, however, is a more recent development. In many of the NIR fluorophore-based imaging studies, a 2 –3-fold difference in signal intensity between affected and control joints was measured. Whether this detection sensitivity is sufficiently robust for extended applications is unknown. It is worth noting that non-targeted NIR-fluorophores tend to accumulate in damaged joints by mechanisms which have yet to be elucidated [19]. In summary, a portfolio of probes with the potential for multiplex imaging in the arthritic joint and other tissues is under development. As inflammatory cell trafficking is a critical (yet incompletely understood) event in early RA and may provide therapeutic opportunities, it follows that inventing probes for molecular imaging in the joint marks a promising development.

Imaging has also aided the delineation of the early stages associated with autoantibody-induced arthritis [30,31]. Wipke *et al.* developed an isotope-labeled, PET-detectable anti-glucose-6-phosphate isomerase IgG [30]. The utilization of antibodies for nuclear imaging is shown in Figure 1. PET revealed uptake of the injected antibody in arthritic joints. Subsequent imaging experiments in mice deficient in C5 or Fc receptors (FcRs), neutrophils, or mast cells uncovered that the latter three components, but not C5, were required for antibody homing to the joint [31]. Imaging in mice deficient in FcR or complement network was also used to identify determinants of joint proteolysis. Ji *et al.* showed that elevated protease activity in the arthritic joint depends on FcRs as well as C5 by utilizing a NIR fluorophore-labeled poly-L-lysine backbone probe that gains fluorescence through protease-mediated enzymatic cleavage [32]. At present, only these studies have applied imaging to mice deficient in genes implicated in musculoskeletal biology. Utilizing a single, specific antibody or probe allows for efficient characterization of multiple knock-out models. Clearly, this approach can uncover biology and offers a blueprint for many other studies.

Tissue destruction in arthritis

Tissue degradation is an irreversible consequence of RA and OA. Molecular imaging holds promise for detection of the onset of the tissue degradation cascade through visualization of the molecular events that precede macroscopic tissue destruction. Indeed, imaging based on the protease-activated NIR fluorophore-labeled poly-L-lysine backbone probe detected a specific fluorescence signal in mild-to-moderate OA, a feature important for clinical diagnosis [33]. Taking advantage of the same probe in an RA model, surrogate imaging permitted quantitative monitoring of the therapeutic response to the anti-proliferative RA drug methotrexate [34]. In a later study, it was demonstrated that a NIR fluorophore-labeled annexin V conjugate can be used for direct imaging of methotrexate-induced apoptosis in the arthritic joint [35]. Reactive oxygen species were visualized in inflamed joints using a simple chemoluminescence reaction [36]. These studies further demonstrated the potential of targeted probes for use in the early detection of arthritis.

Cancer

Imaging has also been utilized to address the progression and potential therapy of skeletal lesions from cancer of the breast [37–44] and prostate [45–52] in addition to other malignancies [53–56]. Experimental metastases were established in mice via intracardiac [37,39–42,44–46,49–50], intraosseous [43,47,48,51–57], or intravenous [38] injection of cancer cells containing different reporter genes, such as FLuc [37,39,40,42–46,49–56] or *Gaussia* luciferase [58] or GFP [38,41,47,48] (Figure 1). In addition to these optical reporter genes, the nuclear reporter gene HSV1 TK was employed [42,58]. A few studies made use of inducible promoters to study signaling cascades, but most utilized constitutive promoters, thereby allowing only detection of the location and formation of tumors. Due to the musculoskeletal focus of this review, we have excluded studies which image skeletal cancer without providing insights into the interaction between the tumor and its skeletal environment.

Cancer progression

To determine the influence of skeletal maturity on the development of metastasis, tumor formation has been imaged in young and old mice and has suggested a positive effect of active bone turnover on the development of metastasis, but further validation is needed [45]. In a more recent imaging study, Schneider *et al.* found that, in adult mice, pre-treatment with intermittent parathyroid hormone (which constituted an anabolic regimen) increased the number of skeletal tumor sites and was also necessary for the formation of tumors in the hind limb [49]. Hirbe *et al.* investigated the consequence of a catabolic stimulus on tumor formation in a model of osteoclastogenesis enhanced by granulocyte colony-stimulating factor [53]. Imaging demonstrated that treatment with growth factors resulted in increased tumor burden.

Kang *et al.* and Serganova *et al.* focused on transforming growth factor β(TGF-β) signaling *in vivo* [42,58]. Utilizing an HSV1 TK or *Gaussia* luciferase imaging reporter gene under the control of a TGF- β-responsive promoter, activation of TGF- β during the development of bone metastases was demonstrated. Consistent with their results, imaging of tumor formation using constitutively expressed GFP or FLuc reporter genes showed that both pharmacological inhibition of TGF- β signaling and delivery of bone morphogenic protein 7 (BMP-7), a candidate antagonist of TGF-β signaling, led to a significant inhibition of growth of skeletal tumors [41,43,51]. Zhang *et al.* employed cancer cells expressing FLuc under the control of a RANKL promoter to demonstrate *in vivo* that TGF-β transiently induces RANKL, which is a known key activator of osteoclast differentiation, thereby linking TGF-β signaling to bone resorption [57]. Taken together, these studies clearly illustrate how integration of molecular imaging can help to decipher signaling cascades by providing the means for *in-vivo* validation.

Cancer therapy

Osteoclasts drive bone resorption in many skeletal tumors and are a prominent therapeutic target. To measure the efficacy of agents blocking bone resorption such as bisphosphonates or osteoprotegerin, reporter gene-based imaging of the location and formation of tumors as described above has been used. Frequently, reporter gene imaging has been complimented by radiographs for the assessment of erosion of osteolytic bone [38,39,46–48,56].

Thudi *et al.*, Mouchess *et al.*, Peyruchaud *et al.*, and Tannehill-Gregg *et al.* examined the effect of the bisphosphonate zoledronic acid on the formation of bone metastases [38,46,55,56]. Two other research groups studied the *in-vivo* efficacy of olpadronate [39,47]. Burton *et al.* investigated administration of pamidronate [48]. All studies, except for the latter, noted an inhibition of osteolysis as detected by anatomical imaging using radiographs.

Optical reporter gene imaging using bioluminescence or fluorescence yielded mixed results among the studies with respect to observed inhibition of tumor growth. However, a direct comparison between the studies is limited because different treatment protocols were employed.

Osteoprotegerin is another potent inhibitor of osteoclastogenesis and thus inhibits bone resorption. Canon *et al* and Miller *et al.* monitored the anti-tumor effect of direct administration of osteoprotegerin-Fc [37,50], whereas Chanda *et al.* and Sims *et al.* delivered osteoprotegerin via systemic gene and cell-mediated delivery, respectively [40,54]. In all cases, imaging confirmed an *in-vivo* anti tumor effect irrespective of the delivery system used. Murray *et al.* utilized imaging to demonstrate efficient *in-vivo* inhibition of tumor growth through the blockage of the macrophage colony-stimulating factor receptor [44] whereas Fritz *et al.* reported optical imaging of inhibition of tumor progression in response to urokinase plasminogen antagonist expression from engineered mesenchymal stem cells (MSCs) [52].

Collectively, bioluminescence and fluorescence imaging of the location and formation of tumors is a widely used tool, particularly in the evaluation of anti-cancer therapies. This is due to the robustness and ease-of-use of the methods as well as the ability to follow animal cohorts non-invasively over time, thus significantly reducing study time and resources. Imaging studies which include the assessment of signaling pathways are of importance because they can directly address the mechanisms of malignant growth; more of such studies are expected in the near future.

Imaging skeletal gene and cell therapy

Imaging has promoted the development and validation of the two major bone repair and regeneration strategies: gene delivery of bone growth factors (with and without biomaterial support) and transfer of naïve or gene-modified MSCs as single therapeutics or supported by biomaterials.

Gene delivery of bone growth factors

A crucial step in any type of gene therapy is the transfer of the therapeutic gene into target cells. Ideally, the gene is delivered in a controlled fashion with high efficiency and minimal toxicity. Imaging can help in the development of gene transfer technology for musculoskeletal applications. Sheyn *et al.* investigated ultrasound-based nonviral gene transfer for bone formation [59]. A plasmid encoding FLuc was sonoporated into the hindlimbs of mice and bioluminescence imaging used to demonstrate transient expression up to two weeks post-sonoporation. Transfection efficiency was lower as compared with electroporation, but additional work is likely to improve the method. Recombinant adeno-associated virus is a more established vehicle for gene transfer, but its application to bone allografts remains challenging, partly due to irregular surface coating. Yazici *et al.* showed that demineralized bone wafers offer improved virus coating as compared with mineralized controls [60]. Despite the enhanced surface coating, bioluminescence imaging after transduction of a FLuc-expressing recombinant adeno-associated virus showed no improvement in *in-vivo* transduction efficiency.

Dunn *et al.* [61] examined adenoviral over-expression of BMP-7 in the vicinity of titanium dental implants. Before determining the therapeutic effect of BMP-7 expression, FLuc-based bioluminescence imaging was used to profile viral gene expression. Taken together, the use of reporter gene-based imaging has evident implications in skeletal gene therapy because it permits *in-vivo* measurement of gene targeting, transduction efficiency, and expression. To further investigate the exceptional osteogenic potency of BMPs, in particular of BMP-2,

Gafni *et al.* assessed the cellular responses after BMP-2 gene transfer [62]. BMP-2 was expressed in a doxycycline-dependent manner in the hindlimb muscle of OC-FLuc mice, and BMP-2-dependent activation of OC expression in skeletal muscle was demonstrated. Such findings are significant because, despite the clinical success of BMP-2, its precise *in-vivo* action is unknown.

Naïve MSCs

MSCs, often in combination with biomaterial support, are a promising tool for musculoskeletal regeneration. Recent years have witnessed a surge in imaging MSCs, but musculoskeletal applications reaching beyond basic visualization experiments are limited. Initially, Leo *et al.* used FLuc-based reporter gene imaging to compare gene expression from different cell types immobilized on scaffolds and placed intervertebrally in rats [63]. In a more detailed study, Olivo *et al.* applied bioluminescence imaging to the temporal characterization of MSCs seeded on biphasic calcium phosphate [64]. Light production was correlated to different cell seeding densities and proliferation capacity. The authors concluded that a threshold number of proliferative MSCs was necessary for effective bone formation in tissue-engineered constructs. Degano *et al.* compared MSCs with adipose tissue-derived MSCs (termed AMSCs) [65]. FLuc-labeled stem cells were seeded onto an osteoconductive scaffold and placed into a calvaria defect. Imaging subsequently revealed better survival of MSCs as compared with AMSCs, suggesting differences between these cell types with respect to their therapeutic potential. Moving beyond the study of implant-immobilized MSCs, Lee *et al.* utilized bioluminescence imaging to follow systemically administered AMSCs in a mouse femur defect model [66]. Imaging data suggested preferential homing to the injured bone. Bioluminescence imaging also helped to provide evidence for the long-term *in-vivo* survival of engrafted skeletal myoblasts derived from embryonic stem cells [67]. All these studies employed reporter gene-based imaging, which has limitations for clinical applications. Arguably easier to translate into diagnostics is *in-vivo* magnetic resonance imaging (MRI) of iron oxide-labeled MSCs for musculoskeletal repair [68]. The principle of this imaging strategy is outlined in Figure 1. Further work will be required to better establish therapeutic potential and imaging feasibility.

MSCs expressing therapeutic genes

The combination of growth factor gene delivery with stem cell therapy is a logical step in the search for more efficient bone regeneration. To compare the efficacy of adenoviral to lentiviral gene delivery, Feeley *et al.* demonstrated expression of FLuc in MSCs alone or co-expressed with BMP-2 [69]. Prolonged expression from the lentivirus construct was observed, but did not manifest itself in increased bone formation as compared with adenoviral expression. In a related study, Hasharoni *et al.* employed locally transplanted MSCs over-expressing BMP-2 in a spine fusion model and confirmed formation of a fusion mass by CT [70]. They then took advantage of the OC-FLuc mouse model to demonstrate host osteocalcin expression through BMP-2, confirming the expected paracrine effect of the growth factor. To further dissect the *in-vivo* biology of BMP-2 bone formation, Aslan *et al.* compared the effect of Dickkopf-3 overexpression on OC transcription in BMP-2-expressing bone precursor cells [71]. Dickkopf-3 was identified as an inhibitor of BMP-2-induced OC expression and a possible player in the regulation of endochondral bone formation. A recent study by Zilberman *et al.* assessed the bone formation capacity of BMP-2-enhanced MSCs at the mineralization stage [72]. Instead of an imaging reporter gene, they conferred imaging visibility through NIR fluorophore-tagged bisphosphonates. FMT showed that formation of new bone occurred within 2 –3 weeks in ectopic muscle ossification and radial bone defect repair (Figure 2c), respectively.

Imaging cellular processes in osteolysis and osteomyelitis

Surgical procedures in orthopedics often require temporary or permanent implantation of biomaterials ranging from bone cement to screws or total joint replacements. A significant clinical problem presents if implants cause the erosion or infection of bone, referred to as osteolysis or osteomyelitis, respectively.

The application of musculoskeletal molecular imaging to osteolysis and osteomyelitis research is emerging. Ren *et al.* studied periprosthetic osteolysis, which can result from a biological response to wear particles [73]. Dynamic bioluminescence imaging revealed that exogenous reporter macrophages are systemically recruited to a bone cement particle-challenged mouse femur (Figure 2d). The authors suggested that this model is useful for the development of therapies aimed at the modulation of macrophage recruitment. Osteolysis can also occur from implant-associated osteomyelitis, and Li *et al.* investigated the effect of stainless-steel pins infected with *Staphylococcus aureus* on murinebone [74]. By modifying the *S. aureus* with the *lux* operon, the bacteria generate bioluminescence in a fashion similar to FLuc (see Figure 1) yet without the need for exogenous D-luciferin. Imaging permitted identification of the peak of bacterial growth. Together with conventional analysis methods, imaging revealed that high metabolic activity corresponded with exponential growth, whereas the low metabolic state was associated with biofilm formation. The authors also showed that bioluminescence imaging could measure therapeutic response to the antibiotic gentamycin. Thus, these data indicate the potential of imaging not only for the study of bacterial *in-vivo* dissemination, but also for the evaluation of novel anti-bacterial treatments.

Conclusions

The strength of musculoskeletal molecular imaging rests in its ability to carry out repeated assessments of *in-vivo* biology in almost real-time. To move the field of musculoskeletal imaging forward, expanding the portfolio of reporter genes, transgenic mice, and probes appears to be important. For accurate *in-vivo* detection and measurement, these novel tools must provide high specificity for their target. Novel imaging-competent transgenic mice should capture musculoskeletal biology in a tissue-, cell-, and pathway-selective manner. Similarly, improved target specificity is required for next-generation activatable probes.

At present, musculoskeletal molecular imaging takes place only in the pre-clinical arena. Most imaging studies assessed in this review were geared towards musculoskeletal destruction. This reflects the urgent need for improved therapies for arthritis and skeletal cancer, as well as the resources dedicated to these diseases. Musculoskeletal molecular imaging also has great potential in conditions which are very difficult to study *ex vivo*, including bone repair and osteolysis. Beyond the basic research arena, the results obtained from imaging biology in pre-clinical animal models could translate into improved clinical care.

Future clinical applications of musculoskeletal molecular imaging are very likely. Judging from the experimental studies summarized in this review, reporter genes and probes are the two main strategies for conferring imaging visibility (Figure 1). Clinical reporter gene-based imaging is hampered by limitations in efficient and controlled gene transfer. Hence, probes are more likely to enter clinical diagnostics, but a broader, more selective probe portfolio is needed, particularly for imaging cartilage and bone biology. The imaging modalities (Table 1) previously used for detection of probes were largely selected empirically. To assess the full potential of clinical molecular imaging, it will be important to systematically compare and identify the combination of probe and imaging method that is most suited for a desired target within a specific musculoskeletal tissue. In the long term, an array of probe/imaging

modality combinations will probably develop. The success of all novel techniques will depend, at least in part, on their clinical impact and cost-effectiveness.

Acknowledgments

We are indebted to Drs. P. Lassota (Boston, USA), C.-C. Glüer (Kiel, Germany), W. Semmler (Heidelberg, Germany), and R. Bhakta (New York, USA) for comments and corrections on the manuscript. Our work is supported by the National Institutes of Health (grant number AR055294 to PMK).

References

1. Blasberg RG, Tjuvajev JG. Molecular-genetic imaging: current and future perspectives. J Clin Invest 2003;111:1620–1629. [PubMed: 12782662]
2. Gross S, Piwnica-Worms D. Spying on cancer: molecular imaging in vivo with genetically encoded reporters. Cancer Cell 2005;7:5–15. [PubMed: 15652745]
3. Massoud TF, Gambhir SS. Molecular imaging in living subjects: seeing fundamental biological processes in a new light. Genes Dev 2003;17:545–580. [PubMed: 12629038]
4. Weissleder R, Mahmood U. Molecular imaging. Radiology 2001;219:316–333. [PubMed: 11323453]
5. Honigman A, et al. Imaging transgene expression in live animals. Mol Ther 2001;4:239–249. [PubMed: 11545615]
6. Iris B, et al. Molecular imaging of the skeleton: quantitative real-time bioluminescence monitoring gene expression in bone repair and development. J Bone Miner Res 2003;18:570–578. [PubMed: 12619943]
7. Silva MJ, et al. In vivo skeletal imaging of 18F-fluoride with positron emission tomography reveals damage- and time-dependent responses to fatigue loading in the rat ulna. Bone 2006;39:229–236. [PubMed: 16533624]
8. Zaheer A, et al. In vivo near-infrared fluorescence imaging of osteoblastic activity. Nat Biotechnol 2001;19:1148–1154. [PubMed: 11731784]
9. Kozloff KM, et al. Noninvasive optical detection of bone mineral. J Bone Miner Res 2007;22:1208–1216. [PubMed: 17488196]
10. Kozloff KM, et al. Non-invasive optical detection of cathepsin K-mediated fluorescence reveals osteoclast activity in vitro and in vivo. Bone 2009;44:190–198. [PubMed: 19007918]
11. Sprague JE, et al. Noninvasive imaging of osteoclasts in parathyroid hormone-induced osteolysis using a 64Cu-labeled RGD peptide. J Nucl Med 2007;48:311–318. [PubMed: 17268030]
12. Ciana P, et al. Engineering of a mouse for the in vivo profiling of estrogen receptor activity. Mol Endocrinol 2001;15:1104–1113. [PubMed: 11435611]
13. Ciana P, et al. In vivo imaging of transcriptionally active estrogen receptors. Nat Med 2003;9:82–86. [PubMed: 12483206]
14. Zhang N, et al. An inducible nitric oxide synthase-luciferase reporter system for in vivo testing of anti-inflammatory compounds in transgenic mice. J Immunol 2003;170:6307–6319. [PubMed: 12794164]
15. Zhang N, et al. Serum amyloid A-luciferase transgenic mice: response to sepsis, acute arthritis, and contact hypersensitivity and the effects of proteasome inhibition. J Immunol 2005;174:8125–8134. [PubMed: 15944321]
16. Carlsen H, et al. In vivo imaging of NF-kappa B activity. J Immunol 2002;168:1441–1446. [PubMed: 11801687]
17. Bennink RJ, et al. Biodistribution and radiation dosimetry of 99mTc-HMPAO-labeled monocytes in patients with rheumatoid arthritis. J Nucl Med 2008;49:1380–1385. [PubMed: 18632808]
18. Chen WT, et al. Arthritis imaging using a near-infrared fluorescence folate-targeted probe. Arthritis Res Ther 2005;7:R310–R317. [PubMed: 15743478]
19. Hansch A, et al. Diagnosis of arthritis using near-infrared fluorochrome Cy5.5. Invest Radiol 2004;39:626–632. [PubMed: 15377942]

20. Hansch A, et al. In vivo imaging of experimental arthritis with near-infrared fluorescence. Arthritis Rheum 2004;50:961–967. [PubMed: 15022340]
21. Nakajima A, et al. Visualization of antigen-specific T cell in living arthritic mice. J Nippon Med Sch 2006;73:298–299. [PubMed: 17220578]
22. Nakajima A, et al. Antigen-specific T cell-mediated gene therapy in collagen-induced arthritis. J Clin Invest 2001;107:1293–1301. [PubMed: 11375419]
23. Simon GH, et al. Optical imaging of experimental arthritis using allogeneic leukocytes labeled with a near-infrared fluorescent probe. Eur J Nucl Med Mol Imaging 2006;33:998–1006. [PubMed: 16770602]
24. Tarner IH, et al. Retroviral gene therapy of collagen-induced arthritis by local delivery of IL-4. Clin Immunol 2002;105:304–314. [PubMed: 12498812]
25. Turk MJ, et al. Folate-targeted imaging of activated macrophages in rats with adjuvant-induced arthritis. Arthritis Rheum 2002;46:1947–1955. [PubMed: 12124880]
26. Yaghoubi SS, et al. Multimodality imaging of T-cell hybridoma trafficking in collagen-induced arthritic mice: image-based estimation of the number of cells accumulating in mouse paws. J Biomed Opt 2007;12:064025-1–064025-11. [PubMed: 18163841]
27. Nakashima-Matsushita N, et al. Selective expression of folate receptor beta and its possible role in methotrexate transport in synovial macrophages from patients with rheumatoid arthritis. Arthritis Rheum 1999;42:1609–1616. [PubMed: 10446858]
28. Paulos CM, et al. Folate-targeted immunotherapy effectively treats established adjuvant and collagen-induced arthritis. Arthritis Res Ther 2006;8:R77. [PubMed: 16646988]
29. McQueen FM, Ostergaard M. Established rheumatoid arthritis – new imaging modalities. Best Pract Res Clin Rheumatol 2007;21:841–856. [PubMed: 17870031]
30. Wipke BT, et al. Dynamic visualization of a joint-specific autoimmune response through positron emission tomography. Nat Immunol 2002;3:366–372. [PubMed: 11896393]
31. Wipke BT, et al. Staging the initiation of autoantibody-induced arthritis: a critical role for immune complexes. J Immunol 2004;172:7694–7702. [PubMed: 15187152]
32. Ji H, et al. Arthritis critically dependent on innate immune system players. Immunity 2002;16:157–168. [PubMed: 11869678]
33. Lai WF, et al. Early diagnosis of osteoarthritis using cathepsin B sensitive near-infrared fluorescent probes. Osteoarthritis Cartilage 2004;12:239–244. [PubMed: 14972341]
34. Wunder A, et al. In vivo imaging of protease activity in arthritis: a novel approach for monitoring treatment response. Arthritis Rheum 2004;50:2459–2465. [PubMed: 15334458]
35. Wunder A, et al. Methotrexate-induced accumulation of fluorescent annexin V in collagen-induced arthritis. Mol Imaging 2005;4:1–6. [PubMed: 15967121]
36. Chen WT, et al. Imaging reactive oxygen species in arthritis. Mol Imaging 2004;3:159–162. [PubMed: 15530251]
37. Canon JR, et al. Inhibition of RANKL blocks skeletal tumor progression and improves survival in a mouse model of breast cancer bone metastasis. Clin Exp Metastasis 2008;25:119–129. [PubMed: 18064531]
38. Peyruchaud O, et al. Early detection of bone metastases in a murine model using fluorescent human breast cancer cells: application to the use of the bisphosphonate zoledronic acid in the treatment of osteolytic lesions. J Bone Miner Res 2001;16:2027–2034. [PubMed: 11697798]
39. van der Pluijm G, et al. Interference with the microenvironmental support impairs the de novo formation of bone metastases in vivo. Cancer Res 2005;65:7682–7690. [PubMed: 16140935]
40. Chanda D, et al. Systemic osteoprotegerin gene therapy restores tumor-induced bone loss in a therapeutic model of breast cancer bone metastasis. Mol Ther 2008;16:871–878. [PubMed: 18388919]
41. Bandyopadhyay A, et al. Inhibition of pulmonary and skeletal metastasis by a transforming growth factor-beta type I receptor kinase inhibitor. Cancer Res 2006;66:6714–6721. [PubMed: 16818646]
42. Kang Y, et al. Breast cancer bone metastasis mediated by the Smad tumor suppressor pathway. Proc Natl Acad Sci U S A 2005;102:13909–13914. [PubMed: 16172383]

43. Buijs JT, et al. Bone morphogenetic protein 7 in the development and treatment of bone metastases from breast cancer. Cancer Res 2007;67:8742–8751. [PubMed: 17875715]
44. Murray LJ, et al. SU11248 inhibits tumor growth and CSF-1R-dependent osteolysis in an experimental breast cancer bone metastasis model. Clin Exp Metastasis 2003;20:757–766. [PubMed: 14713109]
45. Kalikin LM, et al. In vivo visualization of metastatic prostate cancer and quantitation of disease progression in immunocompromised mice. Cancer Biol Ther 2003;2:656–660. [PubMed: 14688471]
46. Thudi NK, et al. Zoledronic acid decreased osteolysis but not bone metastasis in a nude mouse model of canine prostate cancer with mixed bone lesions. Prostate 2008;68:1116–1125. [PubMed: 18461562]
47. Yang M, et al. The bisphosphonate olpadronate inhibits skeletal prostate cancer progression in a green fluorescent protein nude mouse model. Clin Cancer Res 2006;12:2602–2606. [PubMed: 16638872]
48. Burton DW, et al. Monitoring of skeletal progression of prostate cancer by GFP imaging, X-ray, and serum OPG and PTHrP. Prostate 2005;62:275–281. [PubMed: 15389781]
49. Schneider A, et al. Bone turnover mediates preferential localization of prostate cancer in the skeleton. Endocrinology 2005;146:1727–1736. [PubMed: 15637291]
50. Miller RE, et al. RANK ligand inhibition plus docetaxel improves survival and reduces tumor burden in a murine model of prostate cancer bone metastasis. Mol Cancer Ther 2008;7:2160–2169. [PubMed: 18606716]
51. Buijs JT, et al. BMP7, a putative regulator of epithelial homeostasis in the human prostate, is a potent inhibitor of prostate cancer bone metastasis in vivo. Am J Pathol 2007;171:1047–1057. [PubMed: 17724140]
52. Fritz V, et al. Antitumoral activity and osteogenic potential of mesenchymal stem cells expressing the urokinase-type plasminogen antagonist amino-terminal fragment in a murine model of osteolytic tumor. Stem Cells 2008;26:2981–2990. [PubMed: 18757301]
53. Hirbe AC, et al. Granulocyte colony-stimulating factor enhances bone tumor growth in mice in an osteoclast-dependent manner. Blood 2007;109:3424–3431. [PubMed: 17192391]
54. Sims TL Jr, et al. Neural progenitor cell-mediated delivery of osteoprotegerin limits disease progression in a preclinical model of neuroblastoma bone metastasis. J Pediatr Surg 2009;44:204–210. discussion 210–211. [PubMed: 19159744]
55. Tannehill-Gregg SH, et al. The effect of zoledronic acid and osteoprotegerin on growth of human lung cancer in the tibias of nude mice. Clin Exp Metastasis 2006;23:19–31. [PubMed: 16715352]
56. Mouchess ML, et al. Multimodal imaging analysis of tumor progression and bone resorption in a murine cancer model. J Comput Assist Tomogr 2006;30:525–534. [PubMed: 16778634]
57. Zhang J, et al. In vivo real-time imaging of TGF-beta-induced transcriptional activation of the RANK ligand gene promoter in intraosseous prostate cancer. Prostate 2004;59:360–369. [PubMed: 15065084]
58. Serganova I, et al. Multimodality imaging of TGF{beta} signaling in breast cancer metastases. FASEB J 2009;23:2662–2672. [PubMed: 19325038]
59. Sheyn D, et al. Ultrasound-based nonviral gene delivery induces bone formation in vivo. Gene Ther 2008;15:257–266. [PubMed: 18033309]
60. Yazici C, et al. The effect of surface demineralization of cortical bone allograft on the properties of recombinant adeno-associated virus coatings. Biomaterials 2008;29:3882–3887. [PubMed: 18590929]
61. Dunn CA, et al. BMP gene delivery for alveolar bone engineering at dental implant defects. Mol Ther 2005;11:294–299. [PubMed: 15668141]
62. Gafni Y, et al. Gene therapy platform for bone regeneration using an exogenously regulated, AAV-2-based gene expression system. Mol Ther 2004;9:587–595. [PubMed: 15093189]
63. Leo BM, et al. In vivo bioluminescent imaging of virus-mediated gene transfer and transduced cell transplantation in the intervertebral disc. Spine 2004;29:838–844. [PubMed: 15082981]

64. Olivo C, et al. In vivo bioluminescence imaging study to monitor ectopic bone formation by luciferase gene marked mesenchymal stem cells. J Orthop Res 2008;26:901–909. [PubMed: 18271011]

65. Degano IR, et al. Bioluminescence imaging of calvarial bone repair using bone marrow and adipose tissue-derived mesenchymal stem cells. Biomaterials 2008;29:427–437. [PubMed: 17950456]

66. Lee SW, et al. Stem cell-mediated accelerated bone healing observed with in vivo molecular and small animal imaging technologies in a model of skeletal injury. J Orthop Res 2008;27:295–302. [PubMed: 18752273]

67. Barberi T, et al. Derivation of engraftable skeletal myoblasts from human embryonic stem cells. Nat Med 2007;13:642–648. [PubMed: 17417652]

68. Jing XH, et al. In vivo MR imaging tracking of magnetic iron oxide nanoparticle labeled, engineered, autologous bone marrow mesenchymal stem cells following intra-articular injection. Joint Bone Spine 2008;75:432–438. [PubMed: 18448377]

69. Feeley BT, et al. In vivo molecular imaging of adenoviral versus lentiviral gene therapy in two bone formation models. J Orthop Res 2006;24:1709–1721. [PubMed: 16788987]

70. Hasharoni A, et al. Murine spinal fusion induced by engineered mesenchymal stem cells that conditionally express bone morphogenetic protein-2. J Neurosurg Spine 2005;3:47–52. [PubMed: 16122022]

71. Aslan H, et al. Advanced molecular profiling in vivo detects novel function of dickkopf-3 in the regulation of bone formation. J Bone Miner Res 2006;21:1935–1945. [PubMed: 17002559]

72. Zilberman Y, et al. Fluorescence molecular tomography enables in vivo visualization and quantification of nonunion fracture repair induced by genetically engineered mesenchymal stem cells. J Orthop Res 2008;26:522–530. [PubMed: 17985393]

73. Ren PG, et al. Systemic trafficking of macrophages induced by bone cement particles in nude mice. Biomaterials 2008;29:4760–4765. [PubMed: 18824259]

74. Li D, et al. Quantitative mouse model of implant-associated osteomyelitis and the kinetics of microbial growth, osteolysis, and humoral immunity. J Orthop Res 2008;26:96–105. [PubMed: 17676625]

75. Caplan AI, et al. Adult mesenchymal stem cells for tissue engineering versus regenerative medicine. J Cell Physiol 2007;213:341–347. [PubMed: 17620285]

76. Pittenger MF, et al. Multilineage potential of adult human mesenchymal stem cells. Science 1999;284:143–147. [PubMed: 10102814]

77. Gambhir SS, et al. Imaging adenoviral-directed reporter gene expression in living animals with positron emission tomography. Proc Natl Acad Sci U S A 1999;96:2333–2338. [PubMed: 10051642]

78. Tjuvajev JG, et al. Noninvasive imaging of herpes virus thymidine kinase gene transfer and expression: a potential method for monitoring clinical gene therapy. Cancer Res 1996;56:4087–4095. [PubMed: 8797571]

79. Contag CH, et al. Visualizing gene expression in living mammals using a bioluminescent reporter. Photochem Photobiol 1997;66:523–531. [PubMed: 9337626]

80. Pichler BJ, et al. Latest advances in molecular imaging instrumentation. J Nucl Med 2008;49 (suppl 2):5S–23S. [PubMed: 18523063]

81. Weissleder R, et al. In vivo imaging of tumors with protease-activated near-infrared fluorescent probes. Nat Biotechnol 1999;17:375–378. [PubMed: 10207887]

82. Weissleder R. Molecular imaging in cancer. Science 2006;312:1168–1171. [PubMed: 16728630]

83. Jaffer FA, et al. Molecular imaging of cardiovascular disease. Circulation 2007;116:1052–1061. [PubMed: 17724271]

84. Hildebrandt IJ, Gambhir SS. Molecular imaging applications for immunology. Clin Immunol 2004;111:210–224. [PubMed: 15137954]

85. Hutchens M, Luker GD. Applications of bioluminescence imaging to the study of infectious diseases. Cell Microbiol 2007;9:2315–2322. [PubMed: 17587328]

86. Biswal S, et al. Molecular imaging: integration of molecular imaging into the musculoskeletal imaging practice. Radiology 2007;244:651–671. [PubMed: 17709823]

87. Mayer-Kuckuk P, Boskey AL. Molecular imaging promotes progress in orthopedic research. Bone 2006;39:965–977. [PubMed: 16843078]

88. Zilberman Y, et al. Bioluminescent imaging in bone. Methods Mol Biol 2008;455:261–272. [PubMed: 18463824]

89. Pichler BJ, et al. Multimodal imaging approaches: PET/CT and PET/MRI. Handb Exp Pharmacol 2008;185 (pt 1):109–132. [PubMed: 18626801]

90. Ntziachristos V, et al. Looking and listening to light: the evolution of whole-body photonic imaging. Nat Biotechnol 2005;23:313–320. [PubMed: 15765087]

91. Weissleder R, Ntziachristos V. Shedding light onto live molecular targets. Nat Med 2003;9:123–128. [PubMed: 12514725]

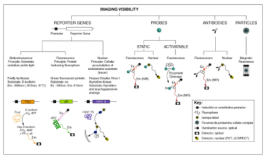

Figure 1.
Strategies for conferring visibility in musculoskeletal molecular imaging. Bioluminescence imaging is frequently based on the *Firefly* luciferase (FLuc) reporter gene. Alternative luciferases used for bioluminescence imaging are *Renilla* or *Gaussia* luciferase, which catalyze the production of CO_2 and light (Em ~480 nm) in a cofactor-independent manner from coelenterazine and its derivatives instead of D-luciferin. The bacterial *lux* operon provides a basis for bioluminescence imaging without the need for exogenous substrate. Other reporter genes are the green fluorescent protein (GFP) for fluorescence imaging as well as the nuclear imaging reporter gene *Herpes simplex* virus 1 thymidine kinase (HSV1 TK), which relies on the preferential phosphorylation and hence cellular trapping of HSV1 thymidine kinase substrates. Employing probes represent a second important strategy for conferring imaging visibility. Two different types of probes can be used: static and activatable. Static probes that have been modified with a fluorophore can be imaged following their *in-vivo* concentration at a target site. Based on the observation that light absorption through biological tissues decreases significantly at wavelengths longer than approximately 600 nm, reaching a minimum around 750 nm [91], near-infrared (NIR, approximately 700 –900 nm) fluorophores are preferred optical labels for fluorescence imaging. Nuclear imaging of isotope-labeled static probes is also an established method. Popular isotopes for imaging applications include the gamma-emitters technetium-99m and indium-111 or the positron emitters fluorine-18 and copper-64. In contrast to static probes, activatable probes gain fluorescence through enzyme-mediated release of active fluorophores from a quenched precursor. Musculoskeletal molecular imaging studies have utilized a probe with a relatively broad selectivity to proteinases, including cathepsin B, L, S, and plasmin [32,33] or a probe preferentially cleaved by cathepsin K [10]. Utilizing antibodies instead of probes is an established strategy and includes fluorophore-labeled antibodies for fluorescence imaging and anti bodies that carry an isotope and thus are suitable for nuclear imaging. Particles composed of a cell membrane-penetrating shell and a paramagnetic iron-oxide core are used for cell labeling and subsequent detection on conventional proton MRI. Abbreviations: Ex, excitation wavelength; Em, emission wavelength; PET, positron emission tomography; γC/ SPECT, gamma camera/single photon emission computed tomography.

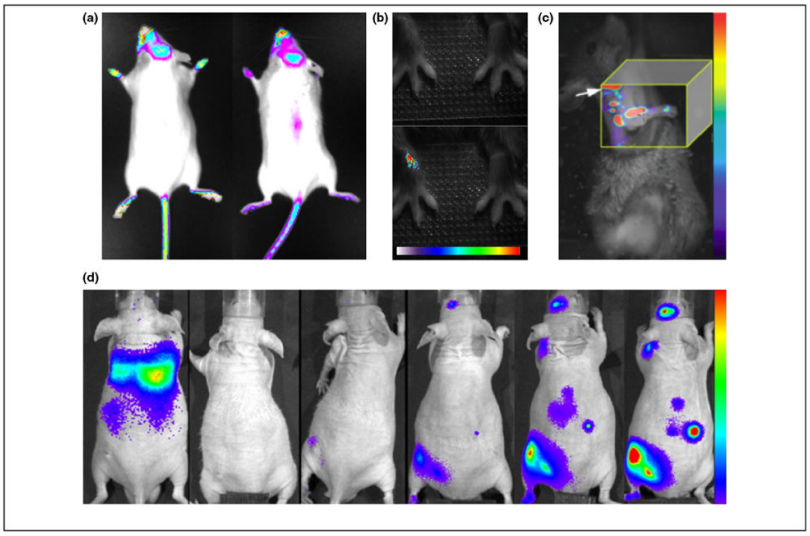

Figure 2.

Applications of musculoskeletal molecular imaging. **(a)** Two representative images of female OC-FLuc transgenic mice at 6–8 weeks of age. Bioluminescence imaging could detect osteocalcin activity in areas of active bone remodeling, including calvaria bones, teeth area, paws and proximal tail vertebra e. Images courtesy of Dr. Yoram Zilberman, Skeletal Biotech Laboratory (Professor Dan Gazit), Hebrew University-Hadassah Medical Center. **(b)** Imaging macrophage infiltration into inflamed joints using a NIR fluorophore-conjugated folate. The top panel shows a white-light image and the bottom panel the merged fluorescence image in which the onset of inflammation was detected 30 h after induction of arthritis in the right wrist. The color bar indicates signal intensity ranging from low (white) to high (red). Reproduced with permission from [18]. **(c)** Fluorescence molecular tomography of bone formation at the mineralization stage utilizing a NIR fluorophore-tagged bisphosphonate. The image shown was acquired 3 weeks after transfer of BMP-2-enhanced MSCs into a radial bone defect and showed a signal along the defect site. The shoulder of the animal is marked by an arrow. The color bar indicates signal intensity ranging from low (violet) to high (red). Reproduced with permission from [72]. **(d)** Temporal-spatial homing of macrophages to a bone cement particle-challenged femur was revealed by a series of bioluminescence images taken every 48 h over 10 days (from left to right). The color bar indicates signal intensity ranging from low (violet) to high (red). Reproduced with permission from [73].

Table 1

Application characteristics of imaging modalities used in musculoskeletal molecular imaging[1]

Feature	Optical imaging		Nuclear imaging [3]	MRI[4]
	Bioluminescence imaging	Fluorescence imaging[2]		
Small animal device[5]	Yes	Yes	Yes	Yes
Sensitivity [6]	High	Moderate	High	Low
Spatial resolution[7]	mm	mm	mm	mm
Detection depth [8]	cm	mm - cm	Not limited	Not limited
Quantitation [9]	Yes	Yes	Yes	In part
Imaging time	sec - min	sec - min	min	min–hours
Anatomical information	No	No	No	Yes
Expenses [10]	Low	Low	High	Moderate
Operator	Self	Self	Self	Self/expert
Investments and infrastructure	Moderate	Low	Very high	High
Clinical modality	No	No	Yes	Yes

[1] Adapted from reference [87].

[2] Surface-weighted imaging (fluorescence reflectance imaging). Fluorescence molecular tomography (FMT) is also available. This method uses multiple point-of-view fluorescence and excitation light measurements. Reconstructed images provide better deep-tissue sensitivity, quantitation accuracy and spatial resolution [90].

[3] PET and gamma camera (γC)/single photon emission computed tomography (SPECT)

[4] Magnetic resonance imaging, extended use in musculoskeletal molecular imaging is anticipated.

[5] Commercially available

[6] Depth-dependent for optical imaging modalities. Estimates have been given for PET (10^{-11}–10^{-12} M), SPECT (10^{-10}–10^{-11} M), MRI (10^{-3}–10^{-5} M), bioluminescence imaging (10^{-15}–10^{-17} M) and fluorescence imaging (10^{-9}–10^{-12} M) [3], however, these values require validation for a particular application.

[7] MRI: Resolution is a function of several parameters, including gradient strength and imaging time; Optical: Spatial resolution is a function of sign al depth.

[8] Values are approximations and dependent upon equipment.

[9] Nuclear imaging and MRI offer excellent, absolute quantitation. Due to heterogeneic light absorption and scattering in biological tissues, quantitation with optical methods is more limited. Most optical imaging instrumentation allows for measurement for relative light emission.

[10] Because of the investments related to molecular imaging, equipment is often available through core facilities. Typical user costs range from $50 –80 per hour for bioluminescence and fluorescence imaging to $150 –200 per hour for PET and MRI. Additional expenses for nuclear imaging may include production or purchase of isotopes and tracer synthesis. Luciferin for bioluminescence imaging costs approximately $2 per mouse.